HHS Public Access

Author manuscript

J Immunol. Author manuscript; available in PMC 2020 November 01.

Published in final edited form as:

J Immunol. 2019 November 01; 203(9): 2415–2424. doi:10.4049/jimmunol.1900484.

TNFα contributes to lymphoid tissue disorganization and GC B cell suppression during intracellular bacterial infection

Maria Popescu[*], **Berenice Cabrera-Martinez**[*], **Gary M. Winslow**[*]

[*]Department of Microbiology and Immunology, Upstate Medical University, Syracuse, NY 13210

Abstract

Bacterial, parasitic, and viral infections are well-known to cause lymphoid tissue disorganization, although the factors, both host and/or pathogen-derived, that mediate these changes are largely unknown. *E. muris* infection in mice causes a loss of germinal center B cells that is accompanied by the generation of extrafollicular T-bet^{+} CD11c^{+} plasmablasts and IgM memory B cells. We addressed a possible role for TNFα in this process, because this cytokine has been shown to regulate germinal center development. Ablation of TNFα during infection resulted in an 8-fold expansion of GL7^{+} CD38^{lo} CD95^{+} germinal center B cells, and a 2.5- and 5-fold expansion of CD138^{+} plasmablasts and T-bet^{+} memory cells, respectively. These changes were accompanied by a reduction in splenomegaly, more organized T and B cell zones, and an improved response to antigen challenge. CXCL13, the ligand for CXCR5, was detected at 6-fold higher levels following infection, but was much reduced following TNFα ablation, suggesting that CXCL13 dysregulation also contributes to loss of lymphoid tissue organization. T_{FH} cells, which also underwent expansion in infected TNFα-deficient mice, may also have contributed to the expansion of T-bet+ B cells, as the latter are known to require T cell help. Our findings contrast with previously described roles for TNFα in GCs, and reveal how host pathogen interactions can induce profound changes in cytokine and chemokine production that can alter lymphoid tissue organization, GC B cell development, and extrafollicular T-bet+ B cell generation.

Introduction

Bacterial, viral, and parasitic infections can all lead to major perturbations of immune homeostasis (1). In many cases, these perturbations are accompanied by excessive inflammation, which can result in disorganization of secondary lymphoid tissues. How B cell differentiation is affected by ongoing inflammatory processes is not well-characterized, but knowledge of lymphocyte differentiation under such conditions is important for understanding how effective humoral immune responses are generated and maintained.

Address correspondence and reprint requests to Dr. Gary Winslow, SUNY Upstate Medical University, 766 Irving Avenue, Syracuse, NY 13210; winslowg@upstate.edu.

Contributions

M.P. conceptualized and executed all of the experiments, analyzed the data, generated figures, and wrote and edited the manuscript. B. C-M. provided essential experimentation and general technical support. G.M.W. aided in the conceptualization of experiments, visualization of the data, and the writing and review of the manuscript.

Data Availability

Data is available upon request.

Histology slides are available online at: https://app.histowiz.com/shared_orders/70a17478-3036-493a-ac0e-b7a54223a443/slides/

Host responses to infections and associated alterations in secondary lymphoid tissues are pathogen-dependent. For example, Salmonella infection leads to the suppression and delay of germinal center (GC) development, via SIP2 T3SS effectors, a process that inhibits bacterial-specific B cell responses (2, 3). During malarial infection, the plasmodium parasite suppresses GC formation by inhibiting the differentiation of T_{FH} cells (4). In contrast, *Trypanosoma brucei* infection induces splenic remodeling and apoptosis of marginal zone B cells, and this remodeling results in a reduction of antibody mediated immunity, and poor control of infection (5). In yet other studies, repeated administration of CpG oligonucleotides was sufficient to cause lymphoid tissue disorganization (6). We have observed similar effects on immunity following infection with the intracellular bacterium *Ehrlichia muris*. We have reported that *E. muris* infection suppresses GC B cell responses, and showed that these changes can inhibit humoral immune responses to foreign antigens (7). Moreover, *E. muris* infection leads to profound IFNγ-dependent hematological changes that mediate extramedullary hematopoiesis, characterized by increases in megakaryocyte-erythrocyte progenitors, common myeloid progenitors, and granulocyte monocyte progenitors in the spleen (8, 9).

Concurrently, *E. muris* infection elicits a robust splenic $CD11c^+$ CD4 T-independent IgM plasmablast response, and generates a large population of long-lived CD4 T-cell-dependent $T\text{-}bet^+$ IgM^+ memory cells (7, 10, 11). These B cells, which are not found in uninfected young C57BL/6 mice, produce pathogen-specific antibodies (12, 13, unpublished data). Unswitched cells dominate this early response to infection, although low frequencies of switched T-bet+ memory B cells are also produced (14). Similar, if not identical, $T\text{-}bet^+$ B cells have been described in a range of chronic conditions, including HIV, HCV (15–17), and malaria infections (18–20), and also in autoimmunity (21–23) and age-related immunity (24, 25). Why and how *E. muris* infection generates such relatively large populations of T-bet+ B cells is unclear, but our previous data suggest that this may be a consequence of the disruptions of normal spleen homeostasis and canonical T cell-B cell interactions.

It is not known whether an inflammatory extrafollicular microenvironment is necessary for the generation of $T\text{-}bet^+$ B cells (26–28), although inflammation is required to induce T-bet expression in T cells (29), and T-bet+ T cells can regulate the inflammatory milieu (30). These observations led us to address a role for inflammatory cytokines in the disruption of immune homeostasis during *E. muris* infection. We focused on TNFα because this cytokine has been previously implicated in GC development and humoral immunity (31–34). In contrast to studies that have described a role for TNFα in GC development under homeostatic conditions, we show that TNFα participates in infection-induced lymphoid disorganization, the disruption of chemokine networks, and the loss of canonical GCs. These findings underscore how bacterial infections can modulate B cell immunity and $T\text{-}bet^+$ B cell ontogeny by modulating host inflammatory responses, in part via TNFα.

Materials and Methods

Mice.—C57BL/6 and TNFα deficient (B6;129S-*Tnf*^{tm1Gkl}/J), mice were obtained from the Jackson Laboratory (Bar Harbor, ME). Mice were used between 6 and 12 weeks of age, and were age-matched across experiments. All animals were bred and/or maintained at SUNY

Upstate Medical University (Syracuse, NY), in accordance with institutional guidelines for animal welfare.

Infections and treatments

Mice were infected via intraperitoneal injection with *E. muris*, at a dose of 5×10^4 copies, as described previously (35). TNFα blockade was achieved by administration of the anti-TNFα mAb XT3.11 (10 mg/kg of body weight, every other day; refs (36, 37), beginning 8 hrs prior to infection and continuing up to, but not including, day 16 post-infection. The isotype-matched Rat IgG1 antibody (clone HRPN) was used as a control; the antibodies were purchased from BioxCell (West Lebanon, NH). CD40L depletion was administered as described elsewhere (11), beginning on day 2 post-infection, every other day, up to day 16 post-infection. CXCL13 was depleted in a similar fashion, using the monoclonal Ab (mAb 5378), which was provided by Vaccinex Inc. (Rochester, NY). Anti-CXCL13 was administered every other day at 30 mg/kg (38), beginning on day 4 post-infection and up to, but not including, day 16 post-infection; an isotype-matched mouse IgG2a antibody (clone 2510) was used as a control.

Flow cytometry and antibodies.—Spleen cells were mechanically disaggregated using a 70 μm cell strainer (BD Biosciences); erythrocytes were removed by hypotonic lysis, using ACK lysing buffer (Quality Biological Inc.). Non-specific binding was blocked by treatment with anti-CD16/32 (2.4G2) prior to incubation with antibodies directed against the following antigens: CD73 (clone TY/11.8, BioLegend), IgM (clone R6–60.2, BD Biosciences), GL7 (clone GL-7, eBioscience), CD19 (clone 6D5, BioLegend), CD11c (clone N418, eBioscience), CXCR5 (clone L138D7, BioLegend), B220 (clone RA3–6B2, BD Biosciences), CD138 (clone 281–2, BD Biosciences) CD38 (clone 90/CD38, BD Biosciences), CD95 (clone Jo2, BD Biosciences), PD-1 (clone RMP1-30, BioLegend), CD3 (clone 17A2, BD Biosciences), CD4 (clone GK1.5, BD Biosciences), CD120a (clone 55R-286, BioLegend), CD120b (clone TR75–89, BioLegend). The cells were stained at 4°C for 20 min, washed, and analyzed for marker expression. Data were acquired on a BD Fortessa flow cytometer using Diva software (BD Biosciences), and were analyzed using FlowJo software (Tree Star, Inc.). CXCL13 was detected in sera from WT and TNFα-deficient mice using the LEGENDplex Proinflammatory Chemokine Mix and Match Subpanel (740097, BioLegend), in accordance with the manufacturer's instructions. Data were acquired on a BD Fortessa flow cytometer with Diva software (BD Biosciences), and were analyzed using the LEGENDplex Data Anaysis Software (BioLegend).

ELISA and ELISpot assays

TNFα concentration in sera was determined using a TNFα ELISA assay (eBioscience 88-7324-22), in accordance with the manufacturer's instructions. Infection-specific IgM and IgG titers were measured by ELISA, using the *E. muris* antigen OMP-19, as previously described (39). The number of antigen-specific IgG and IgM B cells in the spleen was determined using a standard ELISpot assay (40). Spots were imaged using a CTL Series 6 Ultra-V Analyzer (Shaker Height, OH) and enumerated using ImmunoSpot software (Cellular Technology Limited). Spots were normalized to the total population of antibody-secreting cells (ASCs), as determined by flow cytometry.

Immunofluorescence

Spleens were mounted in OCT compound (Tissue-Tek), snap frozen, and sectioned at a thickness of 10 to15 μm. Following a five minute fixation in 4% PFA, samples were transferred to a humidified chamber and blocked and permeabilized for 30 minutes at room temperature, using a 3% non-fat milk solution in 1X PBS with 0.1% IGEPAL CA-630. The antibody panel was separately diluted in blocking buffer and added to the specimens for overnight incubation at 4°C. Prior to mounting, the specimens were stained with a 1 μg/mL DAPI solution (D9542, Sigma) in PBS for five minutes. ProLong Gold antifade mountant was used to affix the sections to glass coverslips. Confocal images were obtained at 20X magnification on a 5×5 tile scan, using an LSM-780 microscope with ZEN imaging software (Zeiss). Images were analyzed using FIJI (41), as necessary, for annotation and cropping. The antibodies used were: AF488-conjugated GL7 (clone GL7), AF594-conjugated CD4 (clone GK1.5), AF647-conjugated CD35 (clone 7E9), AF647-conjugated F4/80 (clone BM8; all from BioLegend), and AF700-conjugated B220 (clone RA3-6B2, BioRad).

Histopathology analyses

Whole spleens were harvested from WT and TNFα deficient mice (n=3 per group per timepoint) at 0 and 16 days post infection and were fixed in 4% paraformaldehyde for 48 hrs at 4°C. Samples were briefly stored in 70% ethanol. Histology analysis was performed by HistoWiz Inc. (Brooklyn, NY), using in-house standard operating procedures and a fully automated workflow. The samples were processed and embedded in paraffin and sectioned at 5μm to generate two slides per collected spleen (3–4 sections per slide). The sections were stained with hematoxylin, dehydrated, and film-coverslipped using a TissueTek-Prisma and Coverslipper apparatus (Sakura). Whole slide scanning was performed using an Aperio AT2 Imaging System (Leica Biosystems). The images were quantified using Halo image analysis software (Indica Labs) with the CytoNuclear module. Samples were diagnosed and evaluated by a HistoWiz pathologist.

Results

Early CD11c^{+} T-bet^{+} memory B cells were detected at much higher frequency in the absence of TNFα, and expressed markers characteristic of GC B cells

Our previous work demonstrated that *E. muris* infection generates both extrafollicular T-bet+ IgM plasmablasts, as well as T-bet+ IgM memory B cells (7, 10, 11). These B cells develop in a unique lymphoid environment, which, in the spleen, lacks conventional B cell follicles and GCs (7). Indeed, inflammation associated with *E. muris* infection likely alters secondary lymphoid homeostasis and contributes to the generation of these B cells, by driving an extrafollicular B cell response. Because TNFα is required for the proper development of B cell follicles and the generation of GCs in immunized mice, we addressed whether this cytokine was, in part, responsible for modulating the lymphoid environment during *E. muris* infection.

TNFα was elicited during *E. muris* infection, as it was detected in peripheral blood, at its highest levels on day 16 post-infection; by day 30, expression had returned to pre-infection levels (Supplementary Figure 1a). To address a role for TNFα during ehrlichial infection, we

first monitored B cell responses in infected WT and TNFα-deficient mice. We identified a small population of $CD19^+$ $GL7^+$ $CD38^{lo}$ $CD95^+$ GC B cells in the spleens of TNFα-deficient mice, as early as day 8 post-infection (Figure 1A, histogram). These GC B cells were also found in infected WT mice on day 16 post-infection, although the cells were much more abundant in the absence of TNFα. We also detected $CD11c^+$ IgM^+ $CD73^+$ B cells on day 16 post-infection, and this population was similarly expanded in the absence of TNFα (Figure 1B). These latter cells likely represent early T-bet+ IgM^+ memory cells (10), as they express surface markers characteristic of that population (e.g., CD73, CD80), as well as T-bet (Supplementary Figure 1b). Approximately 50% of the early $CD11c^+$ $T\text{-}bet^+$ memory cells expressed GL7, characteristic of GC B cells (Figure 1B, right plots). By day 30 post-infection the frequency of $CD11c^+$ $T\text{-}bet^+$ memory cells remained modestly higher in the absence of TNFα. Similar findings were obtained using antibody-mediated ablation of TNFα, indicating that the observations were not a consequence of genetic elimination of the cytokine (Figure 1C).

Follicular structure and lymphoid tissue organization was partially restored in the absence of TNFα

The detection of GC-phenotype B cells in the absence of TNFα in infected mice suggested that B cells were able to develop within GCs, or within an environment that better promoted GC or GC-like B cells. Although changes in follicular architecture have been described in TNFα-deficient mice (31), we observed similar ratios of red and white pulp in both uninfected WT and TNFα-deficient spleens, and these were composed of well-formed follicles (Supplementary Figure 2a). We also observed that GCs, although rare in WT mice, were not detected in TNFα-deficient spleens. On day 16 post-ehrlichial infection, WT mice demonstrated notable white pulp disruption, with approximately 50% of the white pulp either atrophic or disrupted by red pulp elements (Figure 2A). In contrast, infected TNFα-deficient spleens were less disrupted, with only approximately 25% of the white pulp elements atrophic or disrupted. Examination of the intact-appearing white pulp demonstrated that, while the WT group was composed of small to medium-sized lymphoid cells similar to those seen in uninfected mice, the white pulp in TNFα-deficient animals contained medium-sized and large lymphoid cells, reminiscent of centrocytic and centroblastic cells, respectively.

Immunofluorescence analyses revealed that on day 16 post-infection TNFα-deficient mice exhibited discernable follicular structures (Figure 2B). Much better distinction between B and T cell zones was observed, and the B cells formed clusters typical of GCs. In contrast, $GL7^+$ B cells were not readily detected in WT spleens, and B and T cells tended to disperse randomly throughout the tissue, forming noticeably small follicular clusters at a reduced frequency. These data revealed that TNFα in part contributed to the loss of GCs and overall disruption of typical splenic architecture in infected mice.

We also addressed whether splenic disorganization was a consequence of loss or improper distribution of $CD35^+$ FDCs. Although previous studies of TNFα-deficient mice reported that FDCs were absent, we detected FDCs in both uninfected and infected TNFα-deficient mice (Supplementary Figure 2b). However, FDCs were less abundant in TNFα-deficient

mice, relative to uninfected WT mice. FDCs in infected WT mice clustered in the vicinity of overlapping zones of B and T cells; these zones were more discernable in TNFα-deficient spleens. On day 16 post-infection, we detected similar frequencies of FDCs in both WT and TNFα-deficient mice by flow cytometry (Supplementary Figure 2c). Thus, FDCs did not appear to contribute to the microarchitecture differences we observed in the absence of TNFα.

In contrast to the FDCs, we observed much higher frequencies of F4/80^{+} macrophages in TNFα-deficient mice on day 16 post-infection, compared to WT mice, and these macrophages clustered in B cell follicles (Figure 2B). These data also indicated that splenic lymphoid tissue was more organized in the absence of TNFα during infection.

The more structured lymphoid environment in TNFα-deficient mice was also associated with a reduction in splenomegaly, suggesting that the loss of TNFα affected other processes induced by infection, such as extramedullary hematopoiesis (Figure 2C; (42). No apparent changes were detected in bacterial colonization (data not shown), however, which suggests that the effects were likely a consequence of altered inflammatory responses.

TNFα inhibition of GC B cell differentiation was associated with altered CXCL13 expression

We next addressed whether TNFα altered splenic organization by disrupting cell migration and/or positioning, via regulation of chemokine expression. We investigated a role for CXCL13, as this factor is well-known to direct lymphocyte migration and GC development. CXCL13 expression was much higher in serum and spleen cell lysates from WT mice on day 16 post-infection, relative to uninfected mice (Figure 3A). This increase was much reduced in TNFα-deficient mice, although higher levels of CXCL13 were detected, relative to uninfected gene-targeted control mice (Supplementary Figure 1c). We also observed a 10-fold increase in CXCR5 expression on CD11c^{+} B cells from infected TNFα-deficient, but not WT mice (Figure 3B and Supplementary Figure 1d). High CXCR5 expression may be a consequence of the much lower CXCL13 expression in TNFα-deficient mice, due to a reduction in ligand-induced endocytosis in the B cells (43, 44).

To address a role for CXCL13 in TNFα-mediated tissue disorganization, we depleted the chemokine in WT and TNFα-deficient mice, by treating infected mice with an anti-CXCL13 mAb every other day, until day 16 post-infection. Loss of CXCL13 markedly reduced the frequency of GC B cells in both WT and TNFα-deficient mice, although the magnitude of the effect was greater in the absence of TNFα (Figure 3C). This latter outcome was not unexpected, as CXCL13 is known to be required for proper GC development (45, 46). We detected only a modest reduction in CD11c^{+} T-bet^{+} memory B cells in TNFα-deficient mice, although high CXCR5 expression was retained on the B cells. CD11c^{+} B220^{lo} T cell-independent extrafollicular plasmablasts were increased in frequency in the absence of TNFα, although they were unaffected by CXCL13 ablation (Figure 3D). These data suggest that TNFα mediates the suppression of GC B cells in part via the regulation of CXCL13, but that CXCL13 plays at most a modest role in the generation of T-bet^{+} IgM memory cells and plasmablasts. These latter data indicate that normal chemokine cues required for B cell

differentiation in GCs are not necessary for the generation of T cell-independent plasmablasts, or early T-bet^{+} memory cells during ehlichial infection.

GC cell expansion in TNFα-deficient mice required CD40-dependent T cell help and was accompanied by an increase in T_{FH} cells

Differentiation of GC B cells is a T-dependent process, so we next addressed whether TNFα inhibits GC B cells by suppressing T cell helper functions. In this regard, PD-1+ CXCR5+ T_{FH} cells were more abundant in the spleens of infected TNF KO mice on day 16 post-infection, relative to the same population in WT mice (Figure 4A). Among the total T_{FH} population, we detected a higher frequency of GC-phenotype PD-1^{Hi} CXCR5^{Hi} T_{FH} cells under the same conditions. The lower expression of PD-1 and CXCR5 in infected WT mice, relative to uninfected controls, is characteristic of extrafollicular T_{FH} cells (47, 48). These data are consistent with a partial restoration of GC function in the absence of TNFα. T cell-mediated helper functions were required to generate GC B cells in TNFα-deficient mice, as CD40:CD40L blockade reduced the frequency of GC B cells to baseline levels (Figure 4B). These findings reveal that TNFα suppresses GC B cell development, directly or indirectly, by inhibiting T cell helper functions, even in the presence of a large T_{FH} cell response.

CD11c^{+} PBs were also detected at greater frequency in the absence of TNFα

We also examined whether TNFα -deficiency affected the development of CD11c^{+} PBs that are generated in the spleen following *E. muris* infection. CD11c^{+} B220^{low} CD138^{+} plasmablasts were detected at high frequency on day 16 post-infection, as previously reported (7), and these were increased 2.5-fold in frequency in the absence of TNFα (Figure 5A). The antibody-secreting plasmablasts produced ehrlichial outer membrane protein-19 (OMP-19)-specific IgM; however, the number of ASCs was higher in the absence of TNFα (Figure 5B). In contrast, many fewer antigen-specific IgG-secreting B cells were detected, and these were lower in number in the absence of TNFα, presumably as an offset to the expansion of IgM-secreting B cells. We also monitored the number of ASCs five days following challenge of mice on day 50 post-infection with purified OMP-19. The number of IgM-producing, but not IgG-producing, ASCs was greater in TNFα-deficient mice (Figure 5C). These data indicate that TNFα ablation, perhaps by generating higher frequencies of long-term plasma cells or memory cells, can have a long-term effect on the early secondary responses to antigen challenge.

We also addressed whether the increase in IgM-producing cells in the TNFα-deficient mice was CXCL13-dependent, by neutralizing CXCL13, as in the studies shown in Figure 3. In the absence of CXCL13, IgM-producing cells were unaffected on day 16 post-infection; IgG-producing cells were much reduced, as in antibody-treated WT mice (Figure 5D). These data indicated that CXCL13 was responsible for promoting the switched GC-like memory cells, but not the T cell-independent unswitched IgM plasmablasts. CXCL13 ablation did not act indirectly, via T_{FH} cells, however, as CXCL13 blockade in the TNFα KO mice did not affect the frequencies of T_{FH} cells generated during infection (Figure 5E).

Discussion

Inflammatory responses have been extensively described relative to their capacity to direct the quality and magnitude of the host response to infection (49–53). This occurs in part via the regulation of cytokine and chemokine production, which mediate lymphocyte recruitment and differentiation. These inflammatory responses are pathogen-dependent, and differ from those elicited by inert antigens, underscoring the importance of studying immunity in natural infections.

Among the many cytokines produced during infections, TNFα plays a potent immunoregulatory role in the host immune response. TNFα acts to induce pro-inflammatory cytokine signaling, which leads to cytotoxicity, cell proliferation, and NFκB activation (54). Our findings reveal an additional role for TNFα as an important mediator of lymphoid tissue disorganization during bacterial infection. TNFα was in part responsible for mediating tissue disorganization, because blocking TNFα was sufficient to partially restore GC function, and led to the generation of higher frequencies of both T-bet$^+$ plasmablasts and IgM memory B cells. These B cells were sustained for at least as long as 30 days post-infection, and contributed to better recall kinetics upon secondary challenge.

Our finding that TNFα is responsible in part for inhibiting GC or GC-like B cells contrasts with early studies using the TNFα-deficient mice, where the cytokine was shown to be required for the proper development and maintenance of B cell follicles and GCs (31–34). These disparate findings indicate that TNFα function is context-specific, likely a consequence of yet other initiating factors elicited not only the ehrlichiae, but other bacterial, viral, and parasitic infections that cause lymphoid disorganization (1). These pathogens and factors may function in common by generating a cytokine and chemokine “storm” of mediators that include TNFα, and together may cause gross disruptions in lymphoid tissues. How the ehrlichiae trigger innate immunity in this fashion is not known, as these pathogens do not encode classical TLR ligands (55, 56). Nevertheless, the observation that many different infections induce lymphoid tissue disorganization suggests that this process may be of benefit to either the pathogen or host. It would be of obvious benefit to pathogens to limit GC B cell development, and the consequent generation of a high-affinity class-switched immunoglobulin response. However, *E. muris* generates under these same conditions highly effective unswitched B cell responses composed of both early IgM plasmablasts, and long-term T-bet$^+$ IgM memory cells (7, 10). In the absence of evidence to indicate that lymphoid disorganization is caused by the activity of pathogen-derived factors designed to subvert immunity, the most likely explanation is that the lymphoid disorganization we and others have observed results from the loss of positional cues, in part due to chemokine dysregulation.

The overall improved tissue organization we observed suggests that B cells receive more directed positioning cues in the absence of TNFα. In this regard, we detected much higher CXCL13 levels in infected WT mice, relative to uninfected controls. The interaction of CXCL13 with CXCR5 results in migration that is spontaneously random, driven by the search for antigen (46, 57). Established gradients, however, introduce directionality to movement and have been shown to be responsible for proper B cell migration and GC

development (58). Thus, we propose that TNFα, directly or indirectly, induces excess CXCL13 production in infected mice that alters chemokine gradients and leads to the disruption of normal cell migration, and overall follicular and splenic architecture. These dynamics are likely to lead to poor co-stimulatory help, limited BCR engagement, and subsequent inhibition of the GC reaction. Collectively, these changes may be responsible for driving extrafollicular B cell differentiation during *E. muris* infection, which may explain why both T-bet$^+$ plasmablasts and IgM memory cells are produced in such relative abundance during this infection. Depletion of CXCL13 had a minor effect on the generation of early T-bet$^+$ memory cells and plasmablasts in TNFα-deficient mice. Thus, although TNFα may inhibit the generation of GC B cells by inducing excess CXCL13, the cytokine regulates T-bet$^+$ B cell expansion via a CXCL13-independent pathway.

Although we observed and increase in GC-phenotype T-bet+ B cells, this was not accompanied by major changes in either repertoire diversity or mutation frequency (data not shown). We interpret these findings to suggest that the GC-like structures we observed were not fully functional, likely because other components that drive affinity maturation and selection are not intact, even in the absence of TNFα. Our data also suggest that the IgM plasmablasts and T-bet memory cells do not necessarily represent alternative fates, as both populations were found to increase in frequency in the absence of TNFα. Thus, the development of the large unswitched CD11c+ T-bet+ IgM plasmablast population during ehrlichial infection is not solely due to loss of tissue organization and cytokine dysregulation.

Investigation of the roles of TNFα in antimicrobial immunity is an ongoing area of research. TNFα receptors are found on many different immune cells, including B cells. Ablation of TNFR1 or TNFR2 only on B cells did not cause major changes in the frequencies of plasmablasts or memory B cells following infection with *E. muris* (data not shown), indicating that TNFα acts on other cells, perhaps in addition to B cells. TNFα-depletion did not affect the frequency of CD35$^+$ FDCs, however. The lower production of CXCL13 in the absence of TNFα was also associated with high CXCR5 expression on early T-bet$^+$ memory cells. A possible explanation for this observation is that CXCR5 expression is regulated by ligand density and receptor activation (43, 44), such that these dynamics are altered in the absence of TNFα.

Other possible explanations for improved lymphoid tissue organization following TNFα ablation are 1) the apparent large increase in F4/80$^+$ macrophages that was observed in B cell follicles, and 2), the expansion of T_{FH} cells. Splenic macrophages have been shown to be necessary for the generation of T cell-dependent B cell responses and GCs (59), so the increased frequency and follicular organization we observed may have contributed to the increased frequency of GL7$^+$ T-bet$^+$ memory cells that we observed. Moreover, we have demonstrated that CD4 T cells are required for T-bet$^+$ B cell development (10), so TNFα ablation may increase activity by these helper T cells, as has been shown to occur in malarial infection (4). Ehrlichial infection was also associated with increased IFNγ production, and this was further increased in the absence of TNFα, but IFNγ ablation had no apparent effect on either GC B cells, or T-bet$^+$ B cells (data not shown). Thus, both macrophages and T_{FH}

cells may play important roles in TNFα-mediated tissue disorganization, although their exact role has not been resolved.

Our findings that TNFα suppresses GC B cells also contrast with studies of *Listeria monocytogenes*-infected mice, which concluded that TNFα was required for GC development (31, 32). Unlike previously published studies of gene-targeted TNFα deletion, we detected B cell follicles and FDC networks in infected TNFα-deficient mice. It is possible that TNFα has a different effect during listeria infection because this pathogen primarily elicits a CD8 T cell-dependent protective response (60–62). Our findings are, nevertheless, relevant to other infections, including pathogens such as salmonella (3, 63) and plasmodium (4, 64, 65), which are likewise associated with a disordered lymphatic microenvironment and a loss of GCs. A similar role for TNFα in these infections has not been addressed in-depth, however.

Our work supports the notion that host responses to infection may benefit from TNFα inhibition, since we have shown that this treatment generates a higher proportion of both antibody-secreting plasmablasts and IgM memory cells. Alternatively, TNFα inhibition may contribute to autoimmunity by driving auto-reactive B cells, as such B cells have been shown to develop extrafollicularly (28, 66). Autoimmunity induced by anti-TNFα therapy has been documented clinically, although correlations with infections were not reported (67–71). Our findings may warrant a re-interpretation of such studies, especially because T-bet$^+$ B cells have been associated with autoimmunity (21–23).

Supplementary Material

Refer to Web version on PubMed Central for supplementary material.

Acknowledgements

The authors gratefully acknowledge Dr. Michael Lyon for assistance with cryosectioning, and Dr. R. Racine and Ms. Maura Jones for helpful preliminary data. We also acknowledge the excellent technical assistance provided by the SUNY Upstate Medical University's Flow Cytometry and Imaging Core Facilities. We also thank Vaccinex Inc. (Rochester, NY) for generously providing the anti-CXCL13 mAb (clone 5378).

This work was supported by the U.S. Department of Health and Human Services grant R01AI114545 awarded to G.M.W.

References

1. Junt T, Scandella E, and Ludewig B. 2008 Form follows function: lymphoid tissue microarchitecture in antimicrobial immune defence. Nat. Rev. Immunol 2003 3:8 8: 764–775.
2. Cunningham AF, Gaspal F, Serre K, Mohr E, Henderson IR, Scott-Tucker A, Kenny SM, Khan M, Toellner K-M, Lane PJL, and MacLennan ICM. 2007 Salmonella induces a switched antibody response without germinal centers that impedes the extracellular spread of infection. J. Immunol 178: 6200–6207. [PubMed: 17475847]
3. Nanton MR, Lee S-J, Atif SM, Nuccio S-P, Taylor JJ, Bäumler AJ, Way SS, and McSorley SJ. 2014 Direct visualization of endogenous Salmonella-specific B cells reveals a marked delay in clonal expansion and germinal center development. Eur. J. Immunol 45: 428–441. [PubMed: 25346524]
4. Ryg-Cornejo V, Ioannidis LJ, Ly A, Chiu CY, Tellier J, Hill DL, Preston SP, Pellegrini M, Yu Di, Nutt SL, Kallies A, and Hansen DS. 2016 Severe Malaria Infections Impair Germinal Center

Responses by Inhibiting T Follicular Helper Cell Differentiation. Cell Reports 14: 68–81. [PubMed: 26725120]

5. Radwanska M, Guirnalda P, De Trez C, Ryffel B, Black S, and Magez S. 2008 Trypanosomiasis-Induced B Cell Apoptosis Results in Loss of Protective Anti-Parasite Antibody Responses and Abolishment of Vaccine-Induced Memory Responses. PLoS Pathog 4: e1000078–11. [PubMed: 18516300]
6. Heikenwalder M, Polymenidou M, Junt T, Sigurdson C, Wagner H, Akira S, Zinkernagel R, and Aguzzi A. 2004 Lymphoid follicle destruction and immunosuppression after repeated CpG oligodeoxynucleotide administration. Nat. Med 10: 187–192. [PubMed: 14745443]
7. Racine R, Jones DD, Chatterjee M, McLaughlin M, MacNamara KC, and Winslow GM. 2010 Impaired germinal center responses and suppression of local IgG production during intracellular bacterial infection. J. Immunol 184: 5085–5093. [PubMed: 20351185]
8. MacNamara KC, Oduro K, Martin O, Jones DD, McLaughlin M, Choi K, Borjesson DL, and Winslow GM. 2011 Infection-induced myelopoiesis during intracellular bacterial infection is critically dependent upon IFN-signaling. J. Immunol 186: 1032–1043. [PubMed: 21149601]
9. MacNamara KC, Jones M, Martin O, and Winslow GM. 2011 Transient activation of hematopoietic stem and progenitor cells by IFNγ during acute bacterial infection. PLoS ONE 6: e28669–9. [PubMed: 22194881]
10. Yates JL, Racine R, McBride KM, and Winslow GM. 2013 T cell-dependent IgM memory B cells generated during bacterial infection are required for IgG responses to antigen challenge. J. Immunol 191: 1240–1249. [PubMed: 23804710]
11. Papillion AM, Kenderes KJ, Yates JL, and Winslow GM. 2017 Early derivation of IgM memory cells and bone marrow plasmablasts. PLoS ONE. 12: e0178853–17. [PubMed: 28575114]
12. Racine R, Chatterjee M, and Winslow GM. 2008 CD11c expression identifies a population of extrafollicular antigen-specific splenic plasmablasts responsible for CD4 T-independent antibody responses during intracellular bacterial infection. J. Immunol 181: 1375–1385. [PubMed: 18606692]
13. Jones DD, DeIulio GA, and Winslow GM. 2012 Antigen-driven induction of polyreactive IgM during intracellular bacterial infection. J. Immunol 189: 1440–1447. [PubMed: 22730531]
14. Kenderes KJ, Levack RC, Papillion AM, Cabrera-Martinez B, Dishaw LM, and Winslow GM. 2018 T-bet+ IgM memory cells generate multi-lineage effector B cells. Cell Reports 24: 824–837.e3. [PubMed: 30044980]
15. Chang LY, Li Y, and Kaplan DE. 2016 Hepatitis C viraemia reversibly maintains subset of antigen-specific T-bet+ tissue-like memory B cells. J. Viral. Hepat 24: 389–396. [PubMed: 27925349]
16. Knox JJ, Buggert M, Kardava L, Seaton KE, Eller MA, Canaday DH, Robb ML, Ostrowski MA, Deeks SG, Slifka MK, Tomaras GD, Moir S, Moody MA, and Betts MR. 2017 T-bet+ B cells are induced by human viral infections and dominate the HIV gp140 response. JCI Insight 2: S80–16.
17. Knox JJ, Kaplan DE, and Betts MR. 2017 T-bet-expressing B cells during HIV and HCV infections. Cellular Immunol 321: 26–34. [PubMed: 28739077]
18. Weiss GE, Crompton PD, Li S, Walsh LA, Moir S, Traore B, Kayentao K, Ongoiba A, Doumbo OK, and Pierce SK. 2009 Atypical memory B cells are greatly expanded in individuals living in a malaria-endemic area. J. Immunol 183: 2176–2182. [PubMed: 19592645]
19. Obeng-Adjei N, Portugal S, Holla P, Li S, Sohn H, Ambegaonkar A, Skinner J, Bowyer G, Doumbo OK, Traore B, Pierce SK, and Crompton PD. 2017 Malaria-induced interferon-γ drives the expansion of $Tbet^{hi}$ atypical memory B cells. PLoS Pathog 13: e1006576. [PubMed: 28953967]
20. Rivera-Correa J, Guthmiller JJ, Vijay R, Fernandez-Arias C, Pardo-Ruge MA, Gonzalez S, Butler NS, and Rodriguez A. 2017 Plasmodium DNA-mediated TLR9 activation of T-bet+ B cells contributes to autoimmune anaemia during malaria. Nat. Commun 8: 584–11. [PubMed: 28928465]
21. Rubtsova K, Rubtsov AV, Thurman JM, Mennona JM, Kappler JW, and Marrack P. 2017 B cells expressing the transcription factor T-bet drive lupus-like autoimmunity. J. Clin. Invest 127: 1392–1404. [PubMed: 28240602]

22. Liu Y, Zhou S, Qian J, Wang Y, Yu X, Dai D, Dai M, Wu L, Liao Z, Xue Z, Wang J, Hou G, Ma J, Harley JB, Tang Y, and Shen N. 2017 T-bet+ CD11c+ B cells are critical for antichromatin immunoglobulin G production in the development of lupus. Arthritis Res. Ther 19: 481–11.

23. Wang S, Wang J, Kumar V, Karnell JL, Naiman B, Gross PS, Rahman S, Zerrouki K, Hanna R, Morehouse C, Holoweckyj N, Liu H, Autoimmunity Molecular Medicine Team, Manna Z, Goldbach-Mansky R, Hasni S, Siegel R, Sanjuan M, Streicher K, Cancro MP, Kolbeck R, and Ettinger R. 2018 IL-21 drives expansion and plasma cell differentiation of autoreactive CD11chi T-bet+ B cells in SLE. Nat. Commun 9: 1758. [PubMed: 29717110]

24. Hao Y, O'Neill P, Naradikian MS, Scholz JL, and Cancro MP. 2011 A B-cell subset uniquely responsive to innate stimuli accumulates in aged mice. Blood 118: 1294–1304. [PubMed: 21562046]

25. Rubtsov AV, Rubtsova K, Fischer A, Meehan RT, Gillis JZ, Kappler JW, and Marrack P. 2011 Toll-like receptor 7 (TLR7)-driven accumulation of a novel CD11c+ B-cell population is important for the development of autoimmunity. Blood 118: 1305–1315. [PubMed: 21543762]

26. Russell Knode LM, Naradikian MS, Myles A, Scholz JL, Hao Y, Liu D, Ford ML, Tobias JW, Cancro MP, and Gearhart PJ. 2017 Age-associated B cells express a diverse repertoire of VH and Vκ genes with somatic hypermutation. J. Immunol 198: 1921–1927. [PubMed: 28093524]

27. Domeier PP, Chodisetti SB, Soni C, Schell SL, Elias MJ, Wong EB, Cooper TK, Kitamura D, and Rahman ZSM. 2016 IFN-γ receptor and STAT1 signaling in B cells are central to spontaneous germinal center formation and autoimmunity. J. Exp. Med 213: 715–732. [PubMed: 27069112]

28. Jenks SA, Cashman KS, Zumaquero E, Marigorta UM, Patel AV, Wang X, Tomar D, Woodruff MC, Simon Z, Bugrovsky R, Blalock EL, Scharer CD, Tipton CM, Wei C, Lim SS, Petri M, Niewold TB, Anolik JH, Gibson G, Lee FE-H, Boss JM, Lund FE, and Sanz I. 2018 Distinct effector B cells induced by unregulated Toll-like Receptor 7 contribute to pathogenic responses in systemic lupus erythematosus. Immunity 49: 725–739.e6. [PubMed: 30314758]

29. Joshi NS, Cui W, Chandele A, Lee HK, Urso DR, Hagman J, Gapin L, and Kaech SM. 2007 Inflammation directs memory precursor and short-lived effector CD8+ T cell fates via the graded expression of T-bet transcription factor. Immunity 27: 281–295. [PubMed: 17723218]

30. Zimmermann J, Kuhl AA, Weber M, Grun JR,Loffler J, Haftmann C, Riedel R, Maschmeyer P, Lehmann K, Westendorf K, Mashreghi M-F, Lohning M,, Mack A, Radbruch A, and Chang HD 2016 T-bet expression by Th cells promotes type 1 inflammation but is dispensable for colitis. Mucosal Immunol 9: 1487–1499. [PubMed: 26883725]

31. Pasparakis M 1996 Immune and inflammatory responses in TNF alpha-deficient mice: a critical requirement for TNF alpha in the formation of primary B cell follicles, follicular dendritic cell networks and germinal centers, and in the maturation of the humoral immune response. J. Exp. Med 184: 1397–1411. [PubMed: 8879212]

32. Körner H, Cook M, Riminton DS, Lemckert FA, Hoek RM, Ledermann B, Köntgen F, de St Groth BF, and Sedgwick JD. 1997 Distinct roles for lymphotoxin-α and tumor necrosis factor in organogenesis and spatial organization of lymphoid tissue. Eur. J. Immunol 27: 2600–2609. [PubMed: 9368616]

33. Ngo VN, Körner H, Gunn MD, Schmidt KN, Riminton DS, Cooper MD, Browning JL, Sedgwick JD, and Cyster JG. 1999 Lymphotoxin alpha/beta and tumor necrosis factor are required for stromal cell expression of homing chemokines in B and T cell areas of the spleen. J. Exp. Med 189: 403–412. [PubMed: 9892622]

34. Ansel KM, Ngo VN, Hyman PL, Luther SA, Förster R, Sedgwick JD, Browning JL, Lipp M, and Cyster JG. 2000 A chemokine-driven positive feedback loop organizes lymphoid follicles. Nature 406: 309–314. [PubMed: 10917533]

35. Bitsaktsis C, Nandi B, Racine R, MacNamara KC, and Winslow G. 2007 T-cell-independent humoral immunity is sufficient for protection against fatal intracellular ehrlichia infection. Infect. Immun 75: 4933–4941. [PubMed: 17664264]

36. Grinberg-Bleyer Y, Dainichi T, Oh H, Heise N, Klein U, Schmid RM, Hayden MS, and Ghosh S. 2015 Cutting Edge: NF-κB p65 and c-Rel control epidermal development and immune homeostasis in the skin. J. Immunol 194: 2472–2476. [PubMed: 25681334]

37. Zhu EF, Gai SA, Opel CF, Kwan BH, Surana R, Mihm MC, Kauke MJ, Moynihan KD, Angelini A, Williams RT, Stephan MT, Kim JS, Yaffe MB, Irvine DJ, Weiner LM, Dranoff G, and Wittrup

KD. 2015 Synergistic innate and adaptive immune response to combination immunotherapy with anti-tumor antigen antibodies and extended serum half-life IL-2. Cancer Cell 27: 489–501. [PubMed: 25873172]

38. Klimatcheva E, Pandina T, Reilly C, Torno S, Bussler H, Scrivens M, Jonason A, Mallow C, Doherty M, Paris M, Smith ES, and Zauderer M. 2015 CXCL13 antibody for the treatment of autoimmune disorders. BMC Immunol 16: 6–17. [PubMed: 25879435]
39. Shu-yi Li J, Yager E, Reilly M, Freeman C, Reddy GR, Reilly AA, Chu FK, and Winslow GM. 2001 Outer membrane protein-specific monoclonal antibodies protect SCID mice from fatal infection by the obligate intracellular bacterial pathogen ehrlichia chaffeensis. J. Immunol 166: 1855–1862. [PubMed: 11160232]
40. Nandi B, Chatterjee M, Hogle K, McLaughlin M, MacNamara K, Racine R, and Winslow GM. 2009 Antigen display, T-cell activation, and immune evasion during acute and chronic ehrlichiosis. Infect. Immun 77: 4643–4653. [PubMed: 19635826]
41. Schindelin J, Arganda-Carreras I, Frise E, Kaynig V, Longair M, Pietzsch T, Preibisch S, Rueden C, Saalfeld S, Schmid B, Tinevez J-Y, White DJ, Hartenstein V, Eliceiri K, Tomancak P, and Cardona A. 2012 Fiji: an open-source platform for biological-image analysis. Nat. Methods 9: 676–682. [PubMed: 22743772]
42. MacNamara KC, Racine R, Chatterjee M, Borjesson D, and Winslow GM. 2009 Diminished hematopoietic activity associated with alterations in innate and adaptive immunity in a mouse model of human monocytic ehrlichiosis. Infect. Immun 77: 4061–4069. [PubMed: 19451243]
43. Hanyaloglu AC, and Zastrow MV. 2008 Regulation of GPCRs by endocytic membrane trafficking and its potential implications. Annu. Rev. Pharmacol. Toxicol 48: 537–568. [PubMed: 18184106]
44. Pavlos NJ, and Friedman PA. 2017 GPCR signaling and trafficking: the long and short of it. Trends Endocrinol. Metab 28: 213–226. [PubMed: 27889227]
45. Förster R, Mattis AE, Kremmer E, Wolf E, Brem G, and Lipp M. 1996 A putative chemokine receptor, BLR1, directs B cell migration to defined lymphoid organs and specific anatomic compartments of the spleen. Cell 87: 1037–1047. [PubMed: 8978608]
46. Saez de Guinoa J, Barrio L, Mellado M, and Carrasco YR. 2011 CXCL13/CXCR5 signaling enhances BCR-triggered B-cell activation by shaping cell dynamics. Blood 118: 1560–1569. [PubMed: 21659539]
47. Odegard JM, Marks BR, DiPlacido LD, Poholek AC, Kono DH, Dong C, Flavell RA, and Craft J. 2008 ICOS-dependent extrafollicular helper T cells elicit IgG production via IL-21 in systemic autoimmunity. J. Exp. Med 205: 2873–2886. [PubMed: 18981236]
48. Elsner RA, Ernst DN, and Baumgarth N. 2012 Single and coexpression of CXCR4 and CXCR5 Identifies CD4 T helper cells in distinct lymph node niches during influenza virus infection. J. Virol 86: 7146–7157. [PubMed: 22532671]
49. Barton GM 2008 A calculated response: control of inflammation by the innate immune system. J. Clin. Invest 118: 413–420. [PubMed: 18246191]
50. Shteinberg M, Shah A, and Elborn JS. 2019 New insights into immunological responses to infection in bronchiectasis. Eur. Respir. J 53: 1–4.
51. Vincenzo B, Asif IJ, Nikolaos P, and Francesco M. 2015 Adaptive immunity and inflammation. International Journal of Inflammation 2015: 1–1.
52. Seillet C, Belz GT, and Mielke LA. 2014 Complexity of cytokine network regulation of innate lymphoid cells in protective immunity. Cytokine 70: 1–10. [PubMed: 24972988]
53. Al-Banna NA, Cyprian F, and Albert MJ. 2018 Cytokine responses in campylobacteriosis: linking pathogenesis to immunity. Cytokine Growth Factor Rev 41: 75–87. [PubMed: 29550265]
54. Parameswaran N, and Patial S. 2010 Tumor necrosis factor-α signaling in macrophages. Crit. Rev. Eukaryot. Gene Expr 20: 87–103. [PubMed: 21133840]
55. Rikihisa Y 1991 The tribe Ehrlichieae and ehrlichial diseases. Clin. Microbiol. Rev 4: 286–308. [PubMed: 1889044]
56. Lin M, and Rikihisa Y. 2003 Ehrlichia chaffeensis and anaplasma phagocytophilum lack genes for lipid A biosynthesis and incorporate cholesterol for their survival. Infect. Immun 71: 5324–5331. [PubMed: 12933880]

57. Carrasco YR, Fleire SJ, Cameron T, Dustin ML, and Batista FD. 2004 LFA-1/ICAM-1 interaction lowers the threshold of B cell activation by facilitating B cell adhesion and synapse formation. Immunity 20: 589–599. [PubMed: 15142527]
58. Förster R, Mattis AE, Kremmer E, Wolf E, Brem G, and Lipp M. 1996 A putative chemokine receptor, BLR1, directs B cell migration to defined lymphoid organs and specific anatomic compartments of the spleen. Cell. 87: 1037–1047. [PubMed: 8978608]
59. Nikbakht N, Shen S, and Manser T. 2013 Cutting edge: Macrophages are required for localization of antigen-activated B cells to the follicular perimeter and the subsequent germinal center response. J. Immunol 190: 4923–4927. [PubMed: 23567932]
60. North RJ, Dunn PL, and Conlan JW. 1997 Murine listeriosis as a model of antimicrobial defense. Immunol. Rev 158: 27–36. [PubMed: 9314071]
61. Rothe J, Lesslauer W, Lötscher H, Lang Y, Koebel P, Köntgen F, Althage A, Zinkernagel R, Steinmetz M, and Bluethmann H. 1993 Mice lacking the tumour necrosis factor receptor 1 are resistant to TNF-mediated toxicity but highly susceptible to infection by Listeria monocytogenes. Nature. 364: 798–802. [PubMed: 8395024]
62. Bubonja Sonje M, Abram M, Stenzel W, and Deckert M. 2010 Listeria monocytogenes (delta-actA mutant) infection in tumor necrosis factor receptor p55-deficient neonatal mice. Microb. Pathog 49: 186–195. [PubMed: 20685289]
63. Di Niro R, Lee S-J, Vander Heiden JA, Elsner RA, Trivedi N, Bannock JM, Gupta NT, Kleinstein SH, Vigneault F, Gilbert TJ, Meffre E, McSorley SJ, and Shlomchik MJ. 2015 Salmonella infection drives promiscuous B cell activation followed by extrafollicular affinity maturation. Immunity. 43: 120–131. [PubMed: 26187411]
64. Carvalho LJ, Ferreira-da-Cruz MF, Daniel-Ribeiro CT, Pelajo-Machado M, and Lenzi HL. 2007 Germinal center architecture disturbance during plasmodium berghei ANKA infection in CBA mice. Malar. J 6: 327–8.
65. Cadman ET, Abdallah AY, Voisine C, Sponaas AM, Corran P, Lamb T, Brown D, Ndungu F, and Langhorne J. 2008 Alterations of splenic architecture in malaria are induced independently of Toll-Like Receptors 2, 4, and 9 or MyD88 and may affect antibody affinity. Infect. Immun 76: 3924–3931. [PubMed: 18559428]
66. William J, Euler C, Christensen S, and Shlomchik MJ. 2002 Evolution of autoantibody responses via somatic hypermutation outside of germinal centers. Science. 297: 2066–2070. [PubMed: 12242446]
67. Bardazzi F, Odorici G, Virdi A, Antonucci VA, Tengattini V, Patrizi A, and Balestri R. 2014 Autoantibodies in psoriatic patients treated with anti-TNF-α therapy. JDDG: Journal der Deutschen Dermatologischen Gesellschaft. 12: 401–406. [PubMed: 24797746]
68. Ferraro-Peyret C, Coury F, Tebib JG, Bienvenu J, and Fabien N. 2004 Infliximab therapy in rheumatoid arthritis and ankylosing spondylitis-induced specific antinuclear and antiphospholipid autoantibodies without autoimmune clinical manifestations: a two-year prospective study. Arthritis Res. Ther 6: R535–43. [PubMed: 15535831]
69. Oter-López B, Llamas-Velasco M, Sánchez-Pérez J, and Dauden E. 2017 Induction of autoantibodies and autoimmune diseases in patients with psoriasis receiving tumor necrosis factor inhibitors. Actas Dermo-Sifiliográficas (English Edition). 108: 445–456.
70. Atzeni F, Talotta R, Salaffi F, Cassinotti A, Varisco V, Battellino M, Ardizzone S, Pace F, and Sarzi-Puttini P. 2013 Immunogenicity and autoimmunity during anti-TNF therapy. Autoimmun. Rev 12: 703–708. [PubMed: 23207283]
71. de Rycke L, Baeten D, Kruithof E, Van den Bosch F, Veys EM, and de Keyser F. 2005 Infliximab, but not etanercept, induces IgM anti-double-stranded DNA autoantibodies as main antinuclear reactivity: Biologic and clinical implications in autoimmune arthritis. Arthritis Rheum 52: 2192–2201. [PubMed: 15986349]

Key findings

- *E. muris* infection causes major changes in spleen morphology
- The changes in lymphoid tissue organization were in part due to TNFα
- Neutralization of TNFα resulted in an increase in GC-phenotype T-bet+ B cells

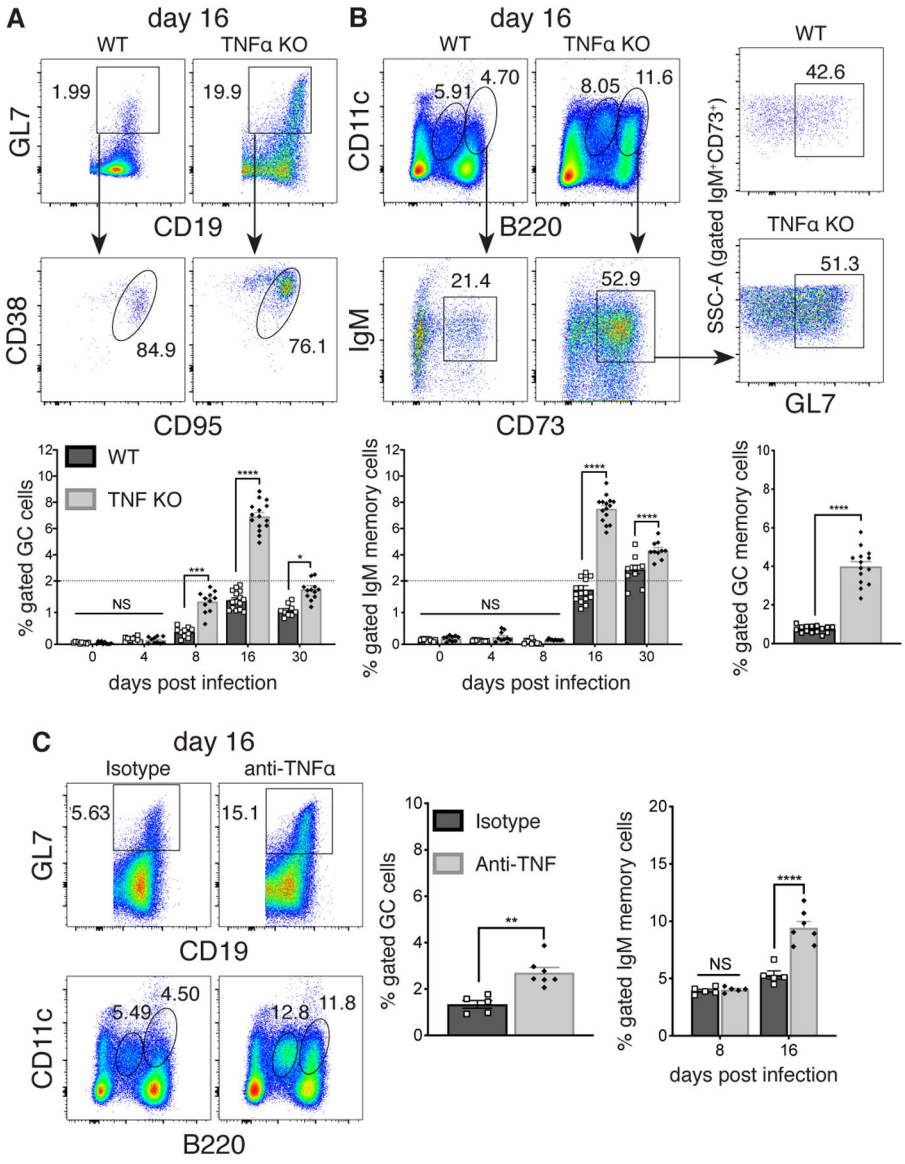

FIGURE 1. Early T-bet+ IgM memory cells underwent expansion and exhibited characteristics of GC B cells in the absence of TNFα

C57BL/6 and congenic TNFα-deficient mice were infected with *E. muris* and B cells were analyzed by flow cytometry on day 16 post-infection. **(A)** Splenic $GL7^+$ $CD19^+$ $CD38^{lo}$ $CD95^+$ B cells were monitored on days 0, 4, 8, 16 and 30 post-infection. Representative flow cytometry dot plots from day 16 post-infection are shown at the top; cumulative data are shown in the plots below. **(B)** $CD11c^+$, $B220^+$, IgM^+, and $CD73^+$ memory cells were also characterized. Representative flow plots and cumulative data are shown on the left; expression of GC markers on CD11c+ CD73+ B cells from WT and TNFα-deficient mice is shown in the right panels.

(C) Mice were administered either an anti-TNFα mAb, or an isotype-matched irrelevant mAb, every other day, for 8 or 16 days following infection, and B cells were analyzed by flow cytometry, as in **A** and **B**. The data in **A-C** were pooled from at least three or more experiments (n=3). Statistical significance was determined in **A** ($p<0.0001$), **B** (bottom left

graph, p<0.0001), and **C** (far right graph, p=0.0001), using a multiple-comparison two-way ANOVA with Tukey's multiple comparison test; or in **B** (bottom right graph, p<0.0001) and **C** (left graph, p=0.0011) using a two-tailed unpaired t-test. All statistical significance is indicated by asterisks (*p>0.03, **p>0.002, ***p>0.0002, ****p<0.0001). The dashed line in the graphs from **A** and **B** indicates a change in the numbering order on the y-axis.

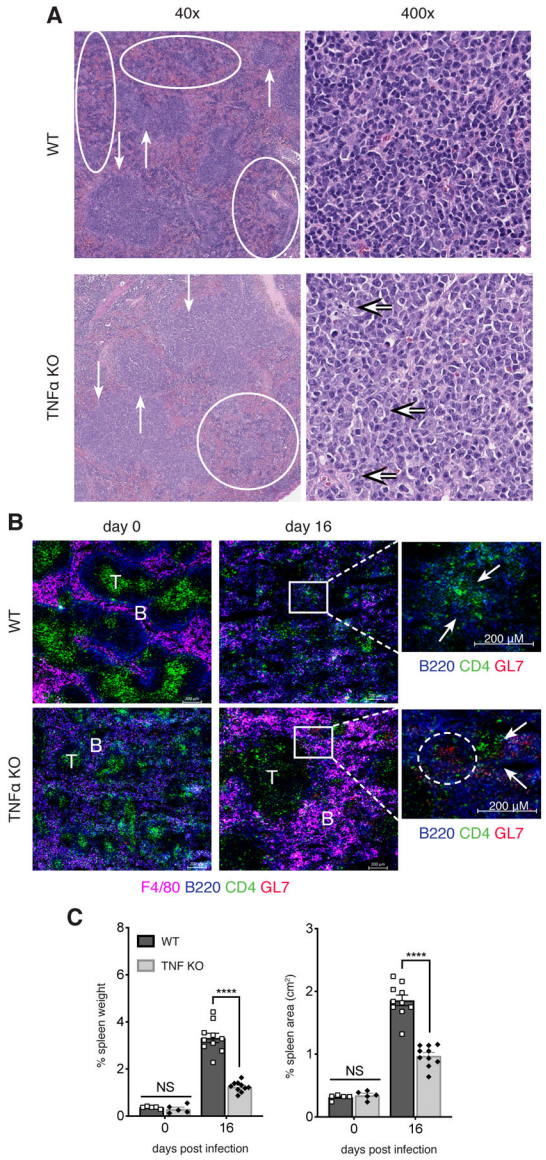

FIGURE 2. TNFα contributed to splenic disorganization during *E. muris* infection.

(A) Paraffin-imbedded spleens from WT and TNFα-deficient mice on day 16 post-infection were analyzed for changes in pathophysiology. In the 40x images, the downward arrows represent areas of intact white pulp, and the upward arrows indicate areas of atrophic white pulp; ovals indicate areas of disrupted white pulp. The 400x images show representative fields for areas of white pulp; in the TNFα-deficient panel, the majority of cells shown were centrocytes; the arrows point to centroblasts. The WT 400x panel was unremarkable. **(B)** Spleens from uninfected (day 0) and day 16 post-infection mice were analyzed for for F4/80 macrophages, B and T cells, and GL7, by immunofluorescence assay. T cell and B cell zones are indicated. Regions of interest on day 16 post-infection are shown at higher magnification; the arrows indicate poorly organized, or distinct T and B cell zones in WT and TNFα-deficient mice, respectively. **(C)** Weight and area of spleens from WT and TNFα-deficient mice are shown. Spleen weight (left graph) was determined as a percent of

body weight; spleen area (right graph) was calculated under the assumption of a rectangular surface, by length and width. The data in **B** were representative of at least three experiments that imaged 2 sections, using groups of three mice. Images in **B** were obtained at 20x magnification and are shown at 100% magnification. The data in **C** were pooled from one or two experiments for days 0 and 16 post-infection, respectively. Statistical significance was determined in **C** ($p<0.0001$ for both) using a multiple-comparison two-way ANOVA with Tukey's multiple comparison test. Statistical significance is indicated by asterisks (*$p>0.03$, **$p>0.002$, ***$p>0.0002$, ****$p<0.0001$).

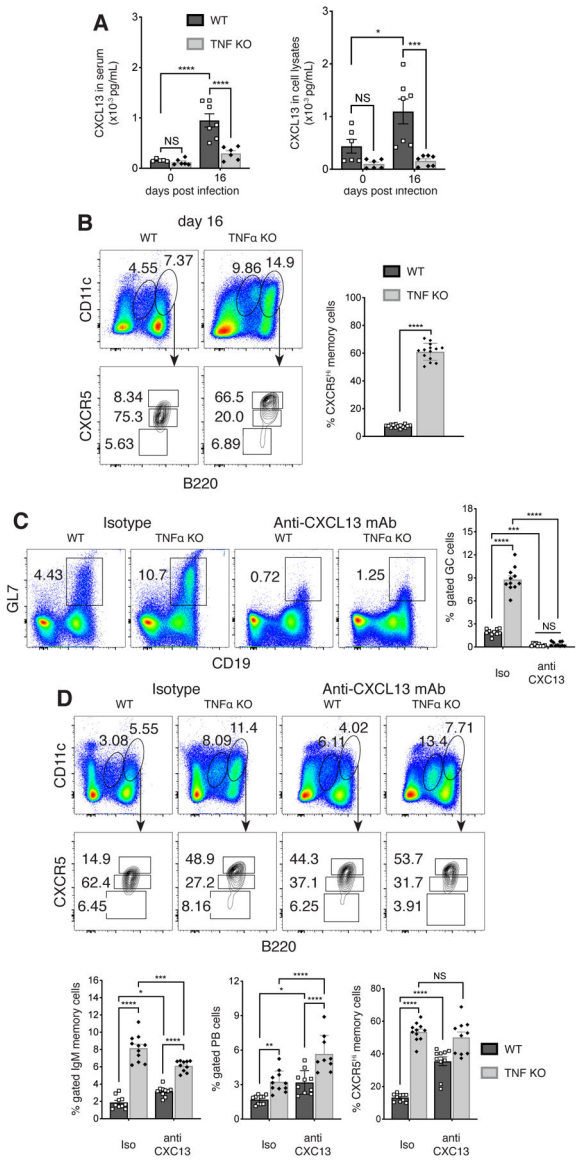

FIGURE 3. CXCL13 was upregulated in response to infection, and limited the expression of GC markers on CD11c$^+$ T-bet$^+$ memory B cells

(A) CXCL13 was quantified by bead-plex-assay in serum (top plot), and splenic cell lysates (bottom plot), that were obtained from uninfected mice, and from infected mice on days 0 and 16 post-infection. **(B)** Expression of CXCR5 in WT and TNFα-deficient mice is shown for CD11c$^+$ early memory B cells on day 16 post-infection (dot plots). Cumulative data are shown on the graph to the right. **(C)** Mice were administered an anti-CXCL13 mAb, or an isotype-matched control mAb, every other day, beginning on day 4 post infection, for as long as 16 days. Representative flow cytometry plots showing of GL7 expression on B cells, among total lymphocytes (top row), and CXCR5 expression on CD11c$^+$ early memory B cells (middle dot plots) are shown for infected anti-CXCL13-treated mice, and untreated controls (iso). Cumulative data is displayed on the bottom row. The data shown were pooled from two or more experiments, where three mice were analyzed per group. Statistical significance was determined in **A** (top: p=0.0017; bottom: p=0.047) and **C** (p<0.0001 for all)

using a multiple-comparison two-way ANOVA with Tukey's multiple comparison test. For the data in **B**, a two-tailed unpaired t-test ($P<0.0001$) was used. All statistical significance is indicated by asterisks (*$p>0.03$, **$p>0.002$, ***$p>0.0002$, ****$p<0.0001$.

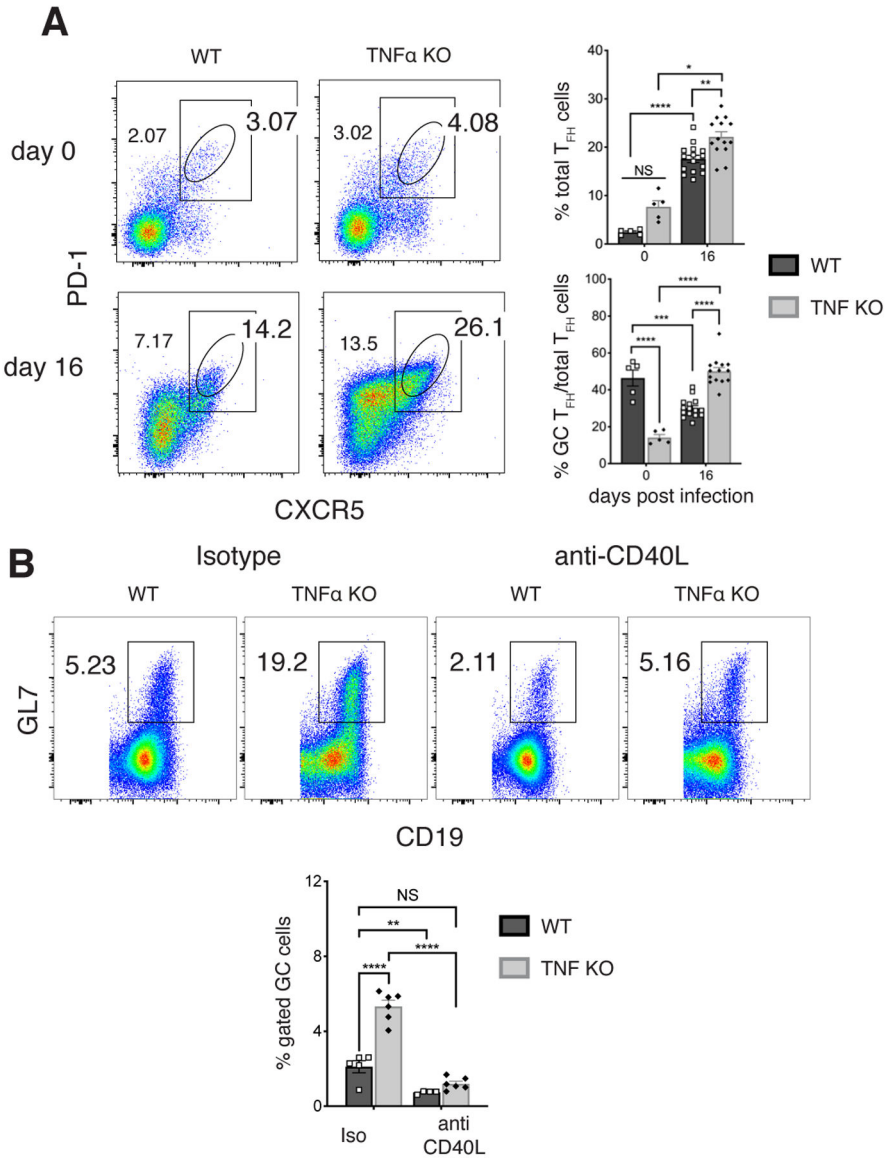

FIGURE 4. T_{FH} cells were found at high frequencies in the absence of TNFα.

(A) $CD4^+$ $CD3^+$ $PD1^+$ $CXCR5^+$ T_{FH} cells were monitored following infection of WT and TNFα-deficient mice. Representative data from day 16 post-infection are shown on the left; cumulative T_{FH} data are shown in the top plot on the right. Also shown (bottom right) is a graph of the proportion of GC T_{FH} cells among total T_{FH} cells. **(B)** Mice were administered an anti-CD40L mAb, or irrelevant isotype-matched mAb, beginning 2 days post-infection, for as long as 16 days. Data from representative control-mAb treated (blue) and anti-CD40L treated (red) mice are shown for both WT and TNFα-deficient groups. Cumulative data are shown in the bottom graph.

Data shown were pooled from at least two experiments, where three mice were used per group. Statistical significance was determined in **A** (top $p<0.0001$, bottom $p<0.0006$) and **B** ($p<0.0001$) using a multiple-comparison two-way ANOVA with Tukey's multiple

comparison test. All statistical significance is indicated by asterisks(*p>0.03, **p>0.002, ***p>0.0002, ****p<0.0001).

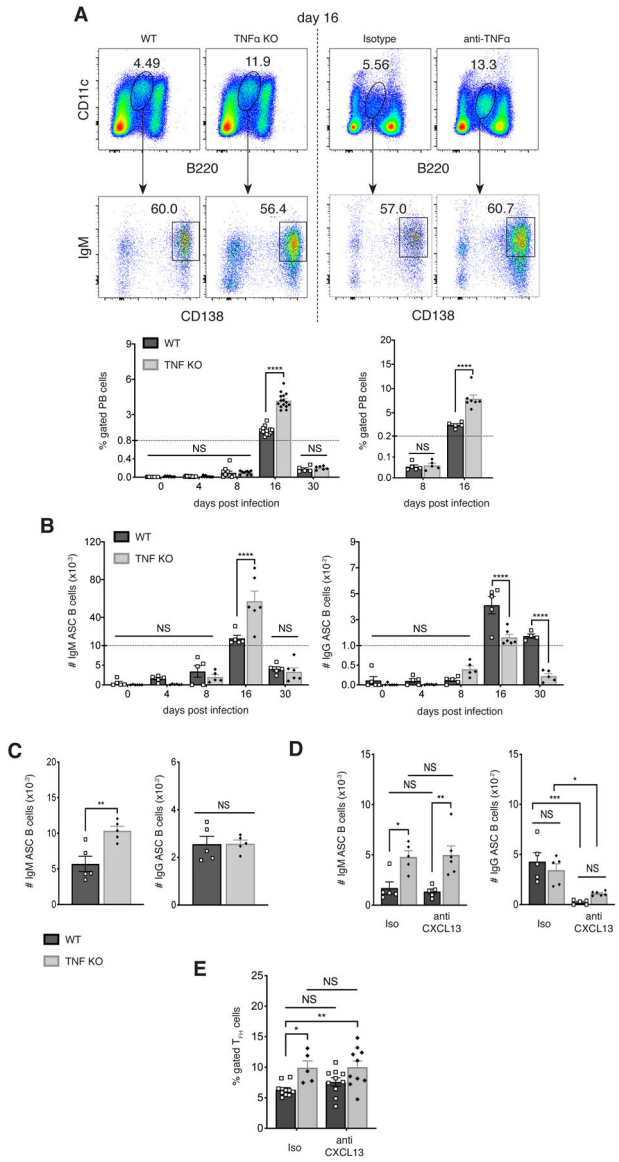

FIGURE 5. CD11c^{+} plasmablasts also underwent expansion in the absence of TNFα, during both primary infection, and following antigen challenge.

(A) CD11c^{+} B220^{lo} IgM^{+} CD138^{+} plasmablasts were monitored in infected wild-type and TNFα-deficient (left panels), or mAb-treated (right panels) mice. Representative data from day 16 post-infection is shown in the top plots, and cumulative data are shown in the graph at the bottom.

(B) The number of IgM (left plot) and IgG (right plot) antigen-specific ASCs was determined by ELISpot assay on the indicated days post-infection. The data were normalized to the total numbers of PBs, as shown in **A**. **(C)** Infected WT and TNFα-deficient mice were challenged 50 days post-infection with purified OMP-19, and the number of IgM (left) and IgG (right) antigen-specific ASCs was determined by ELISpot assay five days following challenge.

(D) WT and TNF-deficient mice were treated with anti-CXCL13 mAb, or an isotype-matched control mAb, every other day, beginning on day 4 post infection, for as long as 16

days. The number of ASCs was determined by ELISpot assay, as in **C**. **(E)** The frequencies of T_{FH} cells in anti-CXCL13-treated WT and TNFα-deficient mice was determined using flow cytometry, as in Figure 4.

The data in **A** and **B** were pooled from at two or more experiment where three mice were analyzed per group. Data in **C and D** were obtained once (n=5). Statistical significance was determined in **A** ($p<0.0001$), **B** ($p<0.0001$) and **D** ($p<0.0001$) using a multiple-comparison two-way ANOVA with Tukey's multiple comparison test. For the data in **C** (IgM: $p=0.0056$; IgG: $p=0.9631$), a two-tailed unpaired t-test was used. All statistical significance is indicated by asterisks (*$p>0.03$, **$p>0.002$, ***$p>0.0002$, ****$p<0.0001$). The dashed line in the graphs in **B** indicates a change in the numbering order on the y-axis.